

## A Facile Approach to Fabrication of ZnO–TiO<sub>2</sub> Hollow Spheres

Mukesh Agrawal,<sup>\*,†</sup> Smrati Gupta,<sup>†,§</sup> Andrij Pich,<sup>‡,||</sup> Nikolaos E. Zafeiropoulos,<sup>†,⊥</sup> and Manfred Stamm<sup>\*,†</sup>

<sup>†</sup>Leibniz-Institut für Polymerforschung Dresden e.V., Hohe Strasse 6, 01069 Dresden, Germany, and  
<sup>‡</sup>Institut für Makromolekulare Chemie, Technische Universität Dresden, Zellescher-Weg 19, 01069 Dresden, Germany. <sup>§</sup>Current Address: Institut für Makromolekulare Chemie, Technische Universität Dresden, Zellescher Weg 19, 01069 Dresden, Germany. <sup>||</sup>Current Address: DWI an der RWTH Aachen e.V., Pauwelsstr. 8, 52056 Aachen, Germany. <sup>⊥</sup>Current Address: Department of Materials Science & Engineering, University of Ioannina, Greece.

Received September 8, 2009

A facile approach for the fabrication of hierarchically nanostructured hollow spheres composed of mixed metal oxides (ZnO–TiO<sub>2</sub>) has been demonstrated. The employed protocol involves coating of the functionalized polystyrene (PS) template beads with the successive layers of ZnO and TiO<sub>2</sub> nanoparticles, respectively, followed by the calcination of resulting PS/ZnO–TiO<sub>2</sub> core shell composite particles at elevated temperature. Scanning electron microscopy (SEM) and transmission electron microscopy (TEM) have been employed to evidence the fabrication of the monodisperse, intact, and closed ZnO–TiO<sub>2</sub> hollow spheres. Presence of both ZnO and TiO<sub>2</sub> phases in the ceramic shell of resulting hollow spheres has been confirmed by electron energy loss mapping analysis. Phase purity of the ZnO and TiO<sub>2</sub> phases of the ceramic shell has been studied by X-ray diffraction analysis. Brunauer–Emmett–Teller (BET) method reveals the specific surface area and the average pore diameter of hollow spheres as 59.63 m<sup>2</sup>/g and 3 nm, respectively. Photocatalytic properties of the fabricated ZnO–TiO<sub>2</sub> hollow spheres has been investigated for the degradation of organic dyes and compared with those of ZnO and TiO<sub>2</sub> hollow spheres.

### Introduction

Hollow spheres represent a fascinating class of the materials, which has attracted an immense interest of the researchers because of their potential applications in wide spectrum of areas.<sup>1</sup> A number of studies have been reported on fabrication of nano- and microscaled hollow spheres and capsules.<sup>2</sup> However, most of them are centered around the synthesis and morphological organizations of phase pure nanobuilding blocks despite the increasing interest in nanocomposites. A few synthetic approaches have been proposed for the preparation of mixed metal oxide systems leading to the so-called “sandwich structures” or “core-shell morphology”.<sup>3</sup>

In addition, some studies have reported on the mixed metal oxides porous particles with different compositions including TiO<sub>2</sub>–In<sub>2</sub>O<sub>3</sub>, ZrO<sub>2</sub>–TiO<sub>2</sub>, and TiO<sub>2</sub>–Ga<sub>2</sub>O<sub>3</sub><sup>4</sup> but fabrication of closed, complete, and intact hollow spheres composed of mixed metal oxides has rarely been explored.<sup>5,6</sup> Needless to mention that hollow spheres with porous shell wall and uniform structural parameters have many folds advantages over porous films or particles in the context of their applications. Unlike to the porous particles, hollow spheres can be used in wide range of potential applications including controlled release of the encapsulated agents, protection of the light sensitive components, artificial cells, as well as nanoreactors/confined reaction vessels.<sup>1</sup> When used as fillers, pigments, or coatings, hollow spheres may also provide some immediate advantages over their porous particles because of their relatively low densities.

Polycrystalline TiO<sub>2</sub> and ZnO both are technologically important materials and are being widely used in a variety

\*To whom correspondence should be addressed. E-mail: agrawal@ipfdd.de; stamm@ipfdd.de.

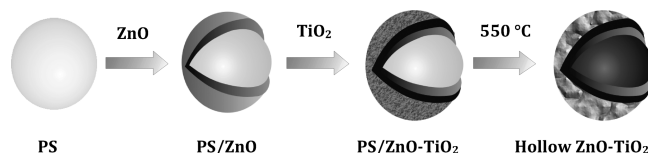
- (1) (a) Caruso, F.; Caruso, R. A.; Mohwald, H. *Science* **1998**, *282*, 1111. (b) Jiang, P.; Bertone, J. F.; Colvin, V. L. *Science* **2001**, *291*, 453. (c) Kim, S. W.; Kim, M.; Lee, W. Y.; Hyeon, T. *J. Am. Chem. Soc.* **2002**, *124*, 7642. (d) Wu, Z.; Yu, K.; Zhang, S.; Xie, Y. *J. Phys. Chem. C* **2008**, *112*, 11307. (e) Wang, Y.; Cai, L.; Xia, Y. *Adv. Mater.* **2005**, *17*, 473. (f) Zhu, Y. F.; Shi, J. L.; Shen, W. H.; Dong, X. P.; Feng, J. W.; Ruan, M. L.; Li, Y. S. *Angew. Chem., Int. Ed.* **2005**, *44*, 5083. (g) Yoon, K. H.; Cho, J.; Kang, D. H. *Mater. Res. Bull.* **1999**, *34*, 1451. (2) (a) Zhong, Z.; Yin, Y.; Gates, B.; Xia, Y. *Adv. Mater.* **2000**, *12*, 206. (b) Yan, C.; Xue, D. *J. Phys. Chem. B* **2006**, *110*, 7102. (c) Sun, X.; Li, Y. *Angew. Chem., Int. Ed.* **2004**, *43*, 3827. (3) (a) Bedja, L.; Kamat, P. V. *J. Phys. Chem.* **1995**, *99*, 9182. (b) Nasr, C.; Hotchandani, S.; Kim, W. Y.; Schmehl, R. H.; Kamat, P. V. *J. Phys. Chem. B* **1997**, *101*, 7480. (c) Di Paola, A.; Palmisano, L.; Derrigo, M.; Augugliaro, V. *J. Phys. Chem. B* **1997**, *101*, 876. (d) Di Paola, A.; Palmisano, L.; Venezia, A. M.; Augugliaro, V. *J. Phys. Chem. B* **1999**, *103*, 8236.

- (4) (a) Shchukin, D. G.; Caruso, R. A. *Chem. Mater.* **2004**, *16*, 2287. (b) Schattka, J. H.; Shchukin, D. G.; Jia, J.; Antonietti, M.; Caruso, R. A. *Chem. Mater.* **2002**, *14*, 5103. (c) Shchukin, D. G.; Schattka, J. H.; Antonietti, M.; Caruso, R. A. *J. Phys. Chem. B* **2003**, *107*, 952. (d) Deshpande, A. S.; Shchukin, D. G.; Ustinovich, E.; Antonietti, M.; Caruso, R. A. *Adv. Funct. Mater.* **2005**, *15*, 239. (5) Wang, W.-W.; Zhu, Y.-J.; Yang, L.-X. *Adv. Funct. Mater.* **2007**, *17*, 59. (6) (a) Zheng, T.; Pang, J.; Tan, G.; He, J.; McPherson, G. L.; Lu, Y.; John, V. T.; Zhan, J. *Langmuir* **2007**, *23*, 5143. (b) Arruebo, M.; Galan, M.; Navascues, N.; Tellez, C.; Marquina, C.; Ibarra, M. R.; Santamaria, J. *Chem. Mater.* **2006**, *18*, 1911.

of applications in liquid–solid as well as in gas–solid regimes.<sup>7</sup> It has been realized that mixed ZnO–TiO<sub>2</sub> polycrystals display profoundly improved physical properties and catalytic activities as compared to the pure ZnO and TiO<sub>2</sub> materials. For example, Lew et al.<sup>8</sup> reported the fabrication of porous and bulky ZnO–TiO<sub>2</sub> mixed metal oxides by pyrolysis–calcination process of citrate precursors and demonstrated enhanced overall performance of ZnO–TiO<sub>2</sub> mixtures over neat ZnO for the desulphurization of coal-derived fuel gases. In another study, Woods et al.<sup>9</sup> reported that addition of TiO<sub>2</sub> reduces the tendency for ZnO reduction and subsequent volatilization of metallic zinc, thereby increasing the maximum sorbent operating temperature. Kim et al.<sup>10</sup> reported that ZnO–TiO<sub>2</sub> films show better performance as dye sensitized solar cell as compared to that of bare TiO<sub>2</sub> film. Similarly, Lin et al.<sup>11</sup> reported 120 times enhancement in the band edge emission of ZnO nanorods after deposition of TiO<sub>2</sub> nanoparticles. These enhancements in most of the properties of ZnO–TiO<sub>2</sub> hybrid materials over the individual ones stem out from the modification in their electronic states. The electron transfer from the conduction band of ZnO to the conduction band of TiO<sub>2</sub> under illumination and, conversely, the hole transfer from the valence band of TiO<sub>2</sub> to the valence band of ZnO give rise to a decrease of the pairs recombination rate leading to an increase in their lifetime.<sup>12</sup> This phenomenon increases the availability of the pairs on the surface of the photocatalyst and consequently an improvement of the occurrence of redox processes can be expected. Apart from alternation of electronic states, the organization pattern and shape of each component in an integrated nanocomposite have also been realized to determine their ultimate physicochemical properties such as chemical reactivity, mass diffusivity, and electro optic activity etc. and thus performance.<sup>13</sup> Therefore it is quite reasonable to explore the fabrication of ZnO–TiO<sub>2</sub> mixed materials with hierarchical morphology.

Herein we report on the fabrication of the hollow spheres composed of mixed ZnO–TiO<sub>2</sub> metal oxides' shell via exploiting the well-known template assisted methodology.<sup>1a,14</sup> The motivation of this study is to design the hollow structures, which can effectively be used in above-mentioned potential applications on the account of the

**Scheme 1. Schematic Presentation of the Fabrication of ZnO–TiO<sub>2</sub> Hollow Spheres**



synergetic effect of the coupling of ZnO with TiO<sub>2</sub> on physical properties and their high porosity and enhanced surface area. The employed process involves coating of polystyrene beads with successive layers of ZnO and TiO<sub>2</sub> nanoparticles in two different steps resulting in the fabrication of PS/ZnO–TiO<sub>2</sub> core–shell composite particles. Subsequently, calcination of these particles at elevated temperature results into the fabrication of monodisperse, closed and porous ZnO–TiO<sub>2</sub> hollow spheres. The schematic presentation of the employed approach is depicted in Scheme 1. In comparison to previously reported studies<sup>15</sup>, the described approach offers an easy, facile, and versatile way to the mixed metal oxides nanostructures.

## Experimental Section

**Materials.** Titanium ethoxide [Ti(OEt)<sub>4</sub>] (85%) and ammonium hydroxide (28–30% NH<sub>3</sub> in water) were purchased from Acros and used without additional purification. Acetic acid (100%) and NaOH (98%) were obtained from Merck and Fluka, respectively, and used as received. Sodium peroxydisulfate (SPDS) (97%), zinc acetate dihydrate (Zn(Ac)<sub>2</sub>·2H<sub>2</sub>O) (99%), 2-propanol (99.5%), rhodamine 6G (99%), and ethanol (99%) all were purchased from Aldrich and have been used without additional purification. Acetoacetoxyethyl methacrylate (AAEM) and styrene (ST) (97%) were purchased from Aldrich and Fluka, respectively, and used after passing through the inhibitor removal column and vacuum distillation. Distilled water was employed as the polymerization medium.

**Synthesis of Polystyrene Beads.** In a typical process, 85 g of water, 9.5 g of styrene and 0.5 g of AAEM were charged into a double-wall glass reactor, equipped with reflux condenser, mechanical stirrer, temperature controller, and nitrogen inlet. After bubbling the nitrogen gas through the reaction media for 30 min, reaction temperature was increased to 70 °C and aqueous SPDS solution (0.15 g in 5 g of water) was added to start the polymerization process. The reaction was allowed to proceed for another 24 h at 70 °C and polystyrene beads as latex with ca. 10% solid content were collected.

**Synthesis of PS/ZnO–TiO<sub>2</sub> Core–Shell Particles.** In first step, a three neck round-bottom flask was charged with 0.11 g of Zn(Ac)<sub>2</sub>·2H<sub>2</sub>O salt and 40 mL of 2-propanol. After stirring at 20 °C for 10 min, temperature was increased to 55 °C and solution was stirred for another 1 h to dissolve the salt. A 2.5 g of the sample of PS latex as prepared above was added into the reaction media with vigorous string during 20 min. Reaction mixture was cooled down to 20 °C and 2 mL of 0.2 M aqueous NaOH solution was added into it. After reacting at 55 °C for another 20 min, solvent was removed under reduced pressure and resulting PS/ZnO particles were well washed with double

- (7) (a) Fierro, J. L. G. In *Metal Oxides: Chemistry and Applications*; CRC Press, Taylor & Francis Group: Boca Raton, FL, 2006; (b) Pelizzetti, E.; Schiavello, M. Eds. *Photochemical Conversion and Storage of Solar Energy*; Kluwer: Dordrecht, 1990; (c) Ollis, D. F.; Al-Ekabi, H. Eds. *Photocatalytic Purification and Treatment of Water and Air*; Elsevier: Amsterdam, 1993.
- (8) Lew, S.; Jothimurugesan, K.; Flytzani-Stephanopoulos, M. *Ind. Eng. Chem. Res.* **1989**, *28*, 535.
- (9) Woods, M. C.; Gangwal, S. K.; Jothimurugesan, K.; Harrison, D. P. *Ind. Eng. Chem. Res.* **1990**, *29*, 1160.
- (10) Kim, K. E.; Jang, S. R.; Park, J.; Vittal, R.; Kim, K. J. *Sol. Energy Mater. Sol. C* **2007**, *91*, 366.
- (11) Lin, H. Y.; Chou, Y. Y.; Cheng, C. L.; Chen, Y. F. *Opt. Express* **2007**, *21*, 13832.
- (12) Serpone, N.; Maruthamuthu, P.; Pichat, P.; Pelizzetti, E.; Hidaka, H. J. *Photochem. Photobiol. A* **1995**, *85*, 247.
- (13) (a) Bell, A. T. *Science* **2003**, *299*, 1688. (b) Valden, M.; Lai, X.; Goodman, D. W. *Science* **1998**, *281*, 1647.
- (14) Agrawal, M.; Pich, A.; Gupta, S.; Zafeiropoulos, N. E.; Simon, P.; Stamm, M. *Langmuir* **2008**, *24*, 1013.

- (15) (a) Kang, Y. C.; Park, S. B. *Mater. Lett.* **1999**, *40*, 129. (b) Kim, J. H.; Choi, W. C.; Kim, H. Y.; Kang, Y.; Park, Y. K. *Powder Technol.* **2005**, *153*, 166. (c) Tian, B.; Li, C.; Gu, F.; Jiang, H.; Hu, Y.; Zhang, J. *Chem. Eng. J* **2009**, *151*, 220. (d) Sutorik, A. C.; Laine, R. M.; Marchal, J.; Johns, T.; Hinklin, T. U.S. Patent 7220398.

distilled water through centrifugation. In second step, 10 mL of extra pure ethanol mixed with 0.025 g of  $\text{Ti}(\text{OEt})_4$  salt was refluxed at 70 °C for 2 hrs and added with 0.05 g of PS/ZnO particles dispersed into the mixture of 0.65 mL water and 2.5 mL of ethanol. After reacting for 20 h, obtained PS/ZnO– $\text{TiO}_2$  composite particles were cleaned by three cycles of centrifugation/redispersion in ethanol and water, respectively, and dried at 35 °C in a vacuum oven. The yields of the PS/ZnO and PS/ZnO– $\text{TiO}_2$  core shell particles have been observed as 81 and 85%, respectively.

**Fabrication of ZnO– $\text{TiO}_2$  Hollow Spheres.** In order to fabricate ZnO– $\text{TiO}_2$  hollow spheres, obtained PS/ZnO– $\text{TiO}_2$  composite particles were calcinated in a furnace at 550 °C for 2 h. Samples were allowed to heat at 5 K/min heating rate from room temperature to 550 °C.

**Photocatalytic Activity of ZnO– $\text{TiO}_2$  Hollow Spheres.** In the photocatalytic experiments, 60 mg of ZnO– $\text{TiO}_2$  hollow sphere were added into 70 mL of aqueous rhodamine 6G solution ( $1 \times 10^{-5}$  M) and reaction mixture was stirred in the dark for 1 h to ensure the adsorption/desorption equilibrium of dye with the hollow spheres. Subsequently, solution was exposed to UV radiations from a high pressure Hg [Xe] lamp at room temperature. The analytic samples exposed to the UV light for different time intervals were taken out from the reaction suspension and filtered off to remove the hollow spheres and analyzed by a UV–visible spectrophotometer to investigate the photodegradation of the rhodamine 6G.

**Characterization.** Transmission electron microscopy (TEM) images were recorded on a Zeiss Omega 912 microscope at 160 kV. Samples were prepared by drying a drop of the dilute solutions of the particles on a carbon grid. In order to prove the presence of both ZnO and  $\text{TiO}_2$  nanoparticles in the shell of hollow spheres, samples were analyzed by elemental mapping image analysis on the same transmission electron microscope. In this analysis, when electron beam is incident into a specimen, a part of the electrons is inelastically scattered and loses a fraction of the energy. The distribution of element in a specimen is clarified by selecting and imaging the electrons with a specific energy loss. A detailed description of the involved phenomena is reported in the literature.<sup>16</sup> Scanning electron microscopy (SEM) images were taken on a Gemini microscope (Zeiss, Germany) at an accelerating voltage of 4 kV. Prior to analysis, samples were coated with thin Au layer to increase the contrast and quality of the images. Particle size measurements were carried out on Zetasizer 2000, Malvern Instruments. The average value of at least three measurements was taken as the particle diameter at room temperature. X-ray scattering patterns were scanned by analyzing the powdery samples on a Seifert XRD 3003 T/T diffractometer using Cu K $\alpha$  monochromatic beam (1.54 Å). FTIR spectra were recorded with Vertex 80 V FTIR spectrometer. Prior to analysis, dried samples were mixed with KBr and pressed into a tablet. Thermo-gravimetric analysis (TGA) was performed on a TGA-7 (Perkin-Elmer) analyzer. Before measurements, samples were dried in vacuum for ca. 48 h and then heated in platinum crucibles at 25–700 °C temperature range with nitrogen as carrier gas at the heating rate of 5° K/min. UV-vis spectra were recorded with a Perkin-Elmer spectrophotometer.

## Results and Discussion

A surfactant-free copolymerization of styrene (ST) and acetoacetoxyethyl methacrylate (AAEM) has been employed for the preparation of polystyrene latex

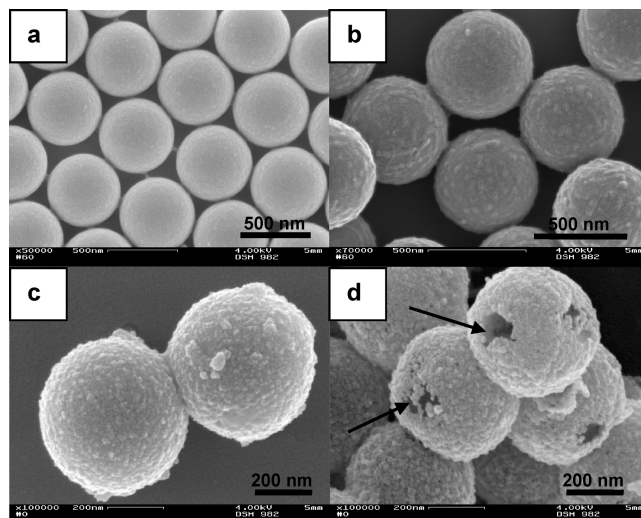


**Figure 1.** SEM images of (a) PS template particles (540 nm), (b) PS/ZnO core-shell composite particles (600 nm) (c) PS/ZnO– $\text{TiO}_2$  core-shell composite particles (705 nm), and (d) ZnO– $\text{TiO}_2$  hollow spheres (650 nm).

particles.<sup>17</sup> The added comonomer AAEM locates predominantly on the surface of emulsion droplets during the copolymerization process and thus stabilizes the obtained colloidal system as well as renders the  $\beta$ -diketone functionality to the surface of resulting PS beads. These functionalities are subsequently exploited to deposit the ZnO nanoparticles on the PS template particles.<sup>18</sup> Figure 1a illustrates SEM image of PS beads used in present study indicating that particles are nearly monodisperse in size with 540 nm diameter and own quite smooth surfaces. Figure 1b shows SEM image of PS/ZnO core-shell composite particles obtained after templating of ZnO nanoparticles against  $\beta$ -diketone functionalized PS beads. This image reveals presence of a complete, homogeneous and smooth ZnO shell on template particles. Moreover, one can observe that average particle diameter has increased from 540 to 600 nm after coating process, indicating precipitation of a 30 nm thick ZnO shell on polystyrene core. Figure 1c illustrates a high magnified SEM micrograph of PS/ZnO– $\text{TiO}_2$  composite particles obtained after coating a titania layer on the surface of PS/ZnO particles. It indicates an increase in average particle diameter from 600 nm for PS/ZnO to 705 nm for PS/ZnO– $\text{TiO}_2$  composite particles. In addition, this SEM image reveals that particles are homogeneous in size and spherical in shape even after the titania coating on previously precipitated ZnO layer. Fabrication of the PS/ZnO composite particles can be attributed to the physical interaction of  $\beta$ -diketone groups located on the surface of the PS beads and  $\text{Zn}^{2+}$  ions formed in reaction media during templating process. It should be mentioned here that ZnO nanoparticles prepared by the employed method have been found to be functionalized with acetate groups.<sup>19</sup> Therefore, it is quite reasonable

(17) Pich, A.; Bhattacharya, S.; Adler, H.-J. P. *Polymer* **2005**, *46*, 1077.

(18) Agrawal, M.; Pich, A.; Zafeiropoulos, N. E.; Gupta, S.; Pionteck, J.; Simon, F.; Stamm, M. *Chem. Mater.* **2007**, *19*, 1845.

(19) Xiong, H.-M.; Zhao, X.; Chen, J.-S. *J. Phys. Chem. B* **2001**, *105*, 10169.

(16) Cardoso, A. H.; Leite, C. A. P.; Galembeck, F. *Langmuir* **1999**, *15*, 4447.



to speculate that deposition of  $\text{TiO}_2$  nanoparticles on ZnO layer has been driven by the physical interaction between carbonyl ( $\text{C}=\text{O}$ ) moieties of acetate groups and  $\text{Ti}^{2+}$  species formed in reaction media during hydrolysis of  $\text{Ti}(\text{OEt})_4$  salt. Figure 1d shows a SEM micrograph of ZnO– $\text{TiO}_2$  hollow spheres obtained after the removal of PS core from PS/ZnO– $\text{TiO}_2$  composite particles. One can observe that calcination of these particles resulted into the fabrication of almost close and intact hollow spheres. It can be attributed to a thick ceramic shell composed of ZnO and  $\text{TiO}_2$  layers, which provided enough mechanical support to these hollow structures to maintain the spherical morphology even after the removal of PS core. It is worth mentioning here that thickness of both the layers can easily be tuned by modulating the concentrations of respective salts in reaction media. Appearance of the holes in the shell of shown hollow spheres can be attributed to the deliberate crushing (by applying force to them) of the sample prior to the SEM analysis to prove their hollow nature.<sup>20</sup> One can clearly see the cavities (shown by arrows) of these hollow structure through these holes. The average diameter of the obtained hollow spheres has been found to be 5–10% less than that of uncalcinated PS/ZnO– $\text{TiO}_2$  particles. It can be attributed to the sintering contraction of nanoparticles or further condensation/polymerization of molecular precursors upon calcination.<sup>21</sup>

Figure 2a and b illustrate TEM images of PS/ZnO– $\text{TiO}_2$  composite particles before and after the calcination process, respectively. In agreement with SEM data, in the case of composite particles a uniform coating of ZnO– $\text{TiO}_2$  composite layer on PS beads can be observed. A noticeable difference in the gray scale of the TEM images of PS/ZnO– $\text{TiO}_2$  composite particles and ZnO– $\text{TiO}_2$  hollow spheres (due to the difference in electron density), confirms that the produced particles are hollow and porous in nature. A close inspection of the TEM image (Figure 2b) of ZnO– $\text{TiO}_2$  hollow spheres reveals presence of individual nanoparticles forming a thick and continuous shell. An overview TEM image and particle size distribution histogram of the ZnO– $\text{TiO}_2$  hollow spheres can be found in Supporting Information (SI) 1. These microscopic results suggest that template assisted fabrication leads to a relatively more definite morphology of mixed metal oxide hollow spheres as compared to those fabricated by alternative methods.<sup>5</sup> In order to further confirm the presence of both ZnO and  $\text{TiO}_2$  nanoparticles in the shell of hollow spheres, samples have been analyzed by electron mapping image analysis, and results are shown in Figure 2c and d. These images have been acquired by visualizing the inelastically scattered electrons in the energy loss windows ( $\Delta E_{\text{loss}}$ ) of 930–1100 eV and 390–464 eV for “Zn” and “Ti” elements, respectively. The red colored areas shown in Figure 2c and d indicate “Zn” and “Ti” enriched areas

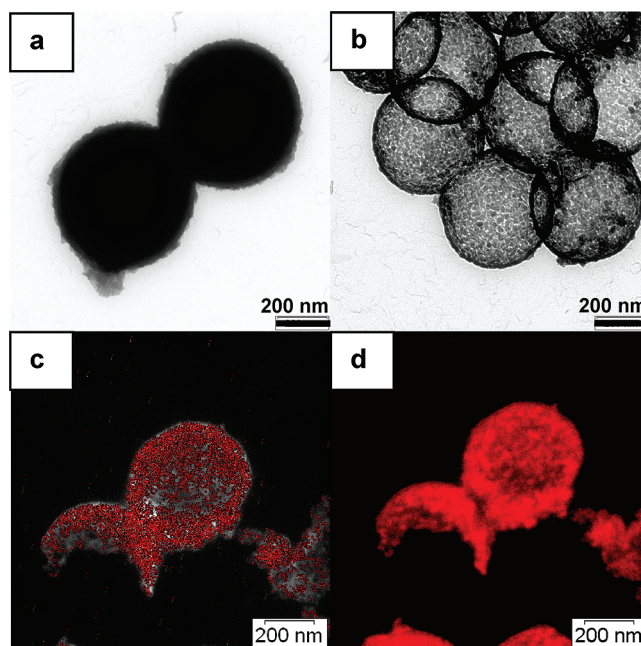


**Figure 2.** TEM images of (a) PS/ZnO– $\text{TiO}_2$  composite particles and (b) ZnO– $\text{TiO}_2$  hollow spheres. Electron energy loss (c) “Zn” and (d) “Ti” element mapping images of ZnO– $\text{TiO}_2$  hollow spheres. In Figure 2c and d, red areas indicate “Zn” and “Ti” enriched parts of hollow spheres, respectively.

of the sample indicating the presence of both ZnO and  $\text{TiO}_2$  in the shell of these hollow spheres.

To investigate the phase purity of the ZnO and  $\text{TiO}_2$  phases of the shell wall, samples have been investigated by XRD analysis and results are shown in SI 2. Surface area and porosity of the fabricated ZnO– $\text{TiO}_2$  hollow spheres have been measured by nitrogen adsorption/desorption isotherms at liquid nitrogen temperature and relative pressures ( $P/P_0$ ) ranging from 0.00 to 1.00. A typical isotherm for as synthesized ZnO– $\text{TiO}_2$  hollow spheres is shown in SI 3a, which reveals a IV type physisorption isotherm with an increase in nitrogen uptake at high relative pressure  $P/P_0 = 0.9$ –1.0 and a wide hysteresis loop indicating a typical mesoporous materials.<sup>22,23</sup> These facts are consistent with the corresponding pore diameter distribution determined by the desorption isotherm (shown in SI 3b), which suggests that sample possesses pore size distribution in the range of 2–4 nm. A close inspection of these results reveals that a fraction of the pores of these hollow spheres lies even in the range of below 2 nm, suggesting the microporous nature of the material. The Brunauer–Emmett–Teller (BET) plot of fabricated ZnO– $\text{TiO}_2$  hollow spheres is depicted in SI 3c. From these results, one can estimate the specific surface area of hollow spheres as 59.63  $\text{m}^2/\text{g}$  using the BET method.<sup>24</sup> Surface area and porosity of these ZnO– $\text{TiO}_2$  hollow spheres are significantly better than those of

- (20) (a) Wang, P.; Chen, D.; Tang, F.-Q. *Langmuir* **2006**, *22*, 4832. (b) Caruso, F.; Caruso, R. A.; Mohwald, H. *Chem. Mater.* **1999**, *11*, 3309. (21) (a) Wang, D.; Caruso, F. *Chem. Mater.* **2002**, *14*, 1909. (b) Wang, L.; Sasaki, T.; Ebina, Y.; Kurashima, K.; Watanabe, M. *Chem. Mater.* **2002**, *14*, 4827.

- (22) Sing, K. S.; Everett, D. H.; Haul, R. A. W.; Moscou, L.; Pieritti, R. A.; Rouquerol, J.; Siemieniowska, T. *Pure Appl. Chem.* **1985**, *57*, 603. (23) Wu, X.; Tian, Y.; Cui, Y.; Wei, L.; Wang, Q.; Chen, Y. *J. Phys. Chem. C* **2007**, *111*, 9704. (24) Brunauer, S.; Emmett, P. H.; Teller, E. *J. Am. Chem. Soc.* **1938**, *60*, 309.

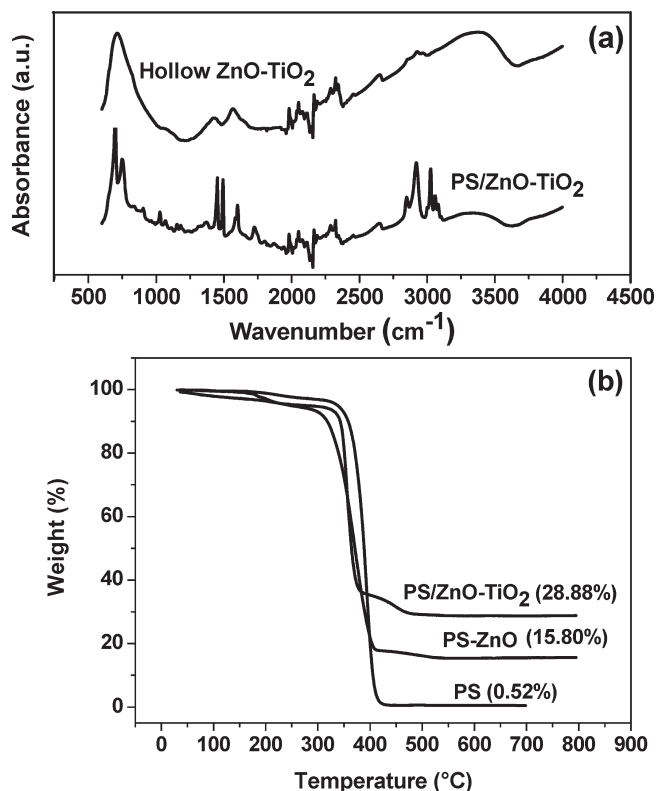


**Figure 3.** (a) FTIR spectra of PS/ZnO-TiO<sub>2</sub> composite particles and ZnO-TiO<sub>2</sub> hollow spheres. (b) TGA scans of neat PS beads, PS/ZnO and PS/ZnO-TiO<sub>2</sub> composite particles.

hollow ZnO spheres, recently reported by Deng et al.<sup>25</sup> Owing to the hollow and porous nature of fabricated hollow spheres, it is quite reasonable to speculate that they can offer comparatively large surface area and hence can work more efficiently in above-mentioned applications as compared to the ZnO-TiO<sub>2</sub> core-shell particles or composite films reported elsewhere.<sup>8,9,26</sup>

The FTIR spectra of PS/ZnO-TiO<sub>2</sub> composite particles and ZnO-TiO<sub>2</sub> hollow spheres are illustrated in Figure 3a. In the case of composite particles, one can notice the presence of aromatic overtones in the range of 1700–2000  $\text{cm}^{-1}$ . In addition, C–H stretching band at around 3000  $\text{cm}^{-1}$ , the aromatic C–C stretching band at around 1470  $\text{cm}^{-1}$ , the C–H out-of-plane band at 765  $\text{cm}^{-1}$ , and the aromatic C–C out-of-plane band at 700  $\text{cm}^{-1}$  can also be observed. All these peaks can be attributed to the PS core of these particles. After the calcinations, all the characteristic peaks of PS have disappeared suggesting the complete removal of polystyrene core from the ZnO-TiO<sub>2</sub> hollow spheres.

In order to study the chemical composition of the ceramic shell of ZnO-TiO<sub>2</sub> hollow spheres, samples have been analyzed by TGA. Figure 3b depicts TGA scans of uncoated, ZnO coated and ZnO-TiO<sub>2</sub> coated PS particles. In all cases, weight loss below 300  $^{\circ}\text{C}$  can be attributed to the evaporation of physically absorbed

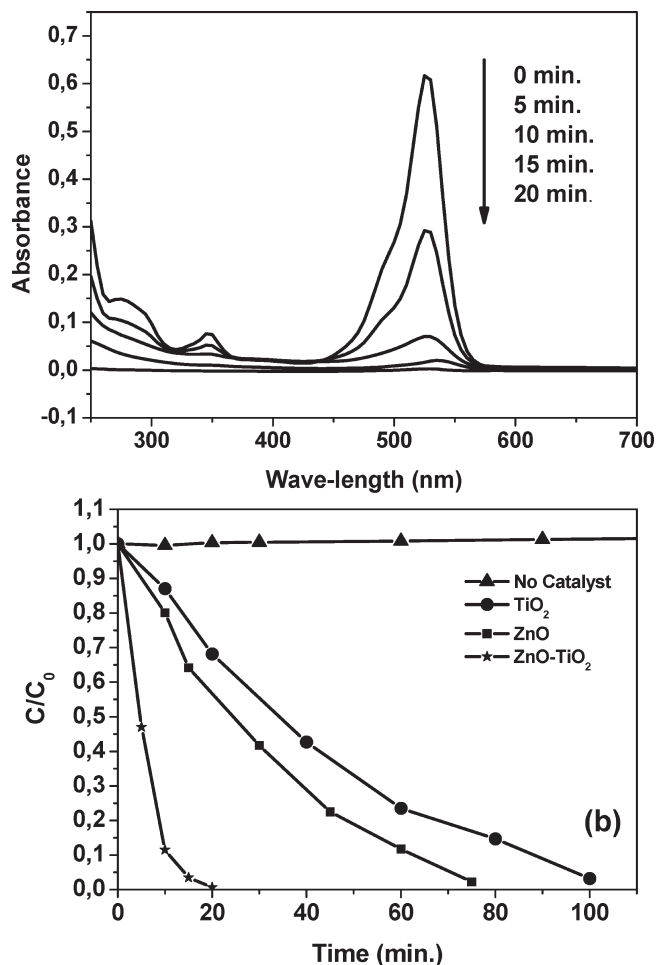


**Figure 4.** (a) UV-vis spectra of the aqueous solutions of rhodamine 6G dye after UV irradiation for different time periods in the presence of ZnO-TiO<sub>2</sub> hollow spheres and (b) photodegradation of the rhodamine 6G dye in the absence of the catalyst and presence of TiO<sub>2</sub>, ZnO and mixed ZnO-TiO<sub>2</sub> hollow spheres.

water and residual solvent of samples. The major weight loss between 325 to 450  $^{\circ}\text{C}$  can be assigned to the loss of PS core. A slight weight loss, which is visible only in the case of ZnO and ZnO-TiO<sub>2</sub> coated polystyrene particles in the range of 460–580  $^{\circ}\text{C}$  can be associated with the decomposition of metal oxide bonded –OH and/or unhydrolysed –OR groups. These data reveal ZnO and TiO<sub>2</sub> contents of PS/ZnO-TiO<sub>2</sub> composite particles as 15.8 and 13.0 wt %, respectively.

To demonstrate the application of fabricated ZnO-TiO<sub>2</sub> hollow spheres, their photocatalytic activity for the degradation of rhodamine 6G dye has been investigated and results are shown in Figure 4. The progress in photodegradation with irradiation time has been monitored by analyzing the UV-visible spectra of reaction solutions, taken out at different time intervals. As shown in Figure 4a, the intensity of the characteristic absorption peak has been found to decrease gradually with increasing the exposure time indicating the photocatalytic degradation of the dye in the presence of ZnO-TiO<sub>2</sub> hollow spheres. In order to evidence the synergetic effect of the coupling of ZnO and TiO<sub>2</sub> metal oxides, rate of the photodegradation of rhodamine 6G,

(25) Deng, Z.; Chen, M.; Gu, G.; Wu, L. *J. Phys. Chem. B* **2008**, *112*, 16.

(26) (a) Hatori, M.; Sasaoka, E.; Uddin, M. A. *Ind. Eng. Chem. Res.* **2001**, *40*, 1884. (b) Kim, D. W.; Lee, S.; Jung, H. S.; Kim, J. Y.; Shin, H.; Hong, K. S. *Int. J. Hydrogen Energ.* **2007**, *32*, 3137.

observed in the presence of mixed metal oxide hollow spheres has been compared with those observed in the presence of  $\text{TiO}_2$  and  $\text{ZnO}$  hollow spheres. Pure  $\text{TiO}_2$  and  $\text{ZnO}$  hollow spheres have been fabricated by the calcination of the  $\text{PS/TiO}_2$  and  $\text{PS/ZnO}$  core shell particles, prepared as described in our previous studies.<sup>27,18</sup>

Figure 4b reveals that organic dye can be photodegraded much faster with mixed  $\text{ZnO-TiO}_2$  metal oxide hollow spheres as compared to those of  $\text{ZnO}$  and  $\text{TiO}_2$  ones. These results succinctly demonstrate that fabricated mixed metal oxide hollow spheres can potentially be used as an efficient photocatalyst for the degradation of organic pollutants. It is worth mentioning here that observed progress in the photodegradation of rhodamine 6G dye in the presence of fabricated  $\text{ZnO-TiO}_2$  hollow spheres is significantly faster than those observed with pure/mixed metal oxide structures reported in the literature.<sup>25,28</sup>

### Conclusions

A template assisted approach for the fabrication of hollow spheres composed of a shell of the  $\text{ZnO-TiO}_2$  mixed metal oxides has been demonstrated. PS beads have been successively coated with  $\text{ZnO}$  and  $\text{TiO}_2$  layers to achieve the  $\text{PS/ZnO-TiO}_2$  hybrid particles. Calcina-

tion of these particles at 550 °C led to the fabrication of closed and intact  $\text{ZnO-TiO}_2$  hollow spheres. Photocatalytic degradation of rhodamine 6G revealed that mixed  $\text{ZnO-TiO}_2$  hollow spheres can work more efficiently as photocatalyst in comparison to pure  $\text{ZnO}$  and  $\text{TiO}_2$  hollow spheres. The presented approach to the fabrication of hollow nanostructures is fast, facile and versatile in nature. The void size of these hollow spheres can effectively be controlled by selecting the PS template particles of suitable diameter. Moreover,  $\text{ZnO}$  or  $\text{TiO}_2$  content as well as shell thickness of these hollow structures can be manipulated by tuning the employed concentration of  $\text{Zn}(\text{Ac})_2 \cdot 2\text{H}_2\text{O}$  and  $\text{Ti}(\text{OEt})_4$  salts in reaction media. In addition, this protocol can be extended for the fabrication of a variety of metal oxides or sulphides hollow spheres such as  $\text{ZnO-ZnS}$ ,  $\text{CdS-ZnS}$ ,  $\text{TiO}_2\text{-CdS}$ , and  $\text{SnO}_2\text{-TiO}_2$ , etc.

**Acknowledgment.** We are thankful to Mrs. Ellen Kern, Mr. Alex Mensch and Dr. Petr Formanek, Dr. Rudiger Hässler, Dr. Victoria Albrecht, and Dr. Dieter Jehnichen for helping out in SEM, TEM, TGA, BET, and XRD measurements, respectively. The authors acknowledge the help from Georgi Paschew, (Technical University, Dresden) in photocatalytic measurements.

**Supporting Information Available:** An overview TEM image and particle size distribution histogram, XRD results, surface area, and porosity measurements of  $\text{ZnO-TiO}_2$  hollow spheres. This material is available free of charge via the Internet at <http://pubs.acs.org>.

(27) Agrawal, M.; Pich, A.; Zafeiropoulos, N. E.; Stamm, M. *Colloid Polym. Sci.* **2008**, *286*, 593.

(28) (a) Xuan, S.; Jiang, W.; Gong, X.; Hu, Y.; Chen, Z. *J. Phys. Chem. C* **2009**, *113*, 553. (b) Shi, X.; Wang, S.; Dong, X.; Zhang, Q. *J. Hazard. Mater.* **2009**, DOI: 10.1016/j.jhazmat.2009.01.038.